Supporting Information

Surfactant-Mediated Ni/MgAl Bifunctional Catalyst for Highly Selective Tandem Conversion of Acetone to Methyl Isobutyl Ketone

Zhongxu Zhang,[a] Shuangshuang Huang,[c] Jingya Sun,[b,] Qiang Yuan,[a,*] Yan Zhu,[a] Xu Liu[a,*]*

[a] School of Chemistry and Chemical Engineering, Nanjing University, Nanjing 210093, China

[b] School of Environmental Science, Nanjing XiaoZhuang University, Nanjing 211171, China

[c] School of Physics and Technology, Wuhan University, Wuhan 430072, China

*Corresponding author: Xu Liu, email: ; Jingya Sun, email: sunjingya@njxzc.edu.cn.

Table of Contents

Experimental Section

Materials. $Al(NO_3)_3 \cdot 9H_2O$, $MgSO_4 \cdot 7H_2O$, sodium hydroxide, anhydrous sodium carbonate, $Ni(NO_3)_2 \cdot 6H_2O$ and acetone, were purchased from Sinopharm Chemical Reagent. SDS and SDBS were purchased from Macklin Biochemical Technology and Bidepharm, respectively. N-heptane was purchased from Aladdin Industrial Corporation. All the chemical reagents were used as received without further purification. Deionized water was used in all the experimental processes.

Preparation of the Mg-Al LDHs. The MgAl LDHs with Mg/Al ratio of 1.5 was prepared by a coprecipitation method. 4.32 g of NaOH and 4.5792 g of Na_2CO_3 were dissolved in 50 mL of deionized water and stirred at 80 ℃. 6.7524 g of $Al(NO_3)_3 \cdot 9H_2O$ and 6.6546 g of $MgSO_4 \cdot 7H_2O$ were introduced into 50 mL of deionized water and stirred at 40 ℃ until all solids were dissolved. The resulting solution was added to the dissolved lye drop by drop and the mixture was stirred at 80 ℃ for 6 h. The precipitate was centrifuged and washed with deionized water several times until the pH reached about 7. The powder of MgAl LDHs was dried at 80 ℃ for 12 h.

Preparation of the Ni/MgAl. Ni supported on MgAl mixed oxides were prepared using ion exchange method. Briefly, 1 g of MgAl LDHs was added to 300 mL of deionized water in a beaker, followed by sonication for 30 min. After stirring for 30 min, the desired amounts of $Ni(NO_3)_2 \cdot 6H_2O$ and either SDS or SDBS were added to the suspension. Note that, the theoretical Ni loading was 10 wt%. And the molar ratio of surfactant to Ni was 10. The mixture was stirred at room temperature for 12 h. Catalyst powders were retained by centrifugation and dried at 80 ℃. The as-synthesized catalysts were reduced using a 5 vol% H_2/Ar stream in a tubular furnace at 450 ℃ for 4 h with a heating rate of 2 ℃·min^{-1}. The catalysts were separately denoted as Ni/MgAl-SDS and Ni/MgAl-SDBS. The preparation of Ni/MgAl catalyst were prepared using the above strategy without surfactant. The MgAl oxides directly generated by MgAl LDHs under the under 450 °C calcination was denoted as MgAl. MgAl, after being modified by SDBS under the same conditions mentioned above, is denoted as MgAl-SDBS.

Catalyst Characterization. XRD patterns of the samples were obtained on a Bruker D8 ADVANCE powder diffractometer using Cu Kα radiation at 40 kV and 40 mA. Element contents of the samples were performed using an Agilent 725-ES Inductively Coupled Plasma-Atomic Emission Spectrometer. N_2 adsorption and desorption experiments were performed with a Micromeritics ASAP 2020 instrument. All samples were degassed under vacuum at 100 ℃ for 5 hours. FTIR was performed using a Vertex70 (Bruker) spectrophotometer with a resolution of 4 cm^{-1}. SEM measurements were taken on a FEI Nova NanoSEM 450 instrument. TEM images were obtained in a FEI Tecnai G^2 F20 instrument. The surface elemental analysis was performed using a Thermo Scientific Nexsa X-ray Photoelectron Spectroscopy equipped with Al Kα radiation. The C_{1s} peak at 284.80 eV was used as a calibration peak.

For H_2-D_2 exchange, 100 mg catalyst was pretreated in an Ar atmosphere (30 mL·min^{-1}) for 30 min at 160 ℃, then cooled to room temperature. 5 vol% H_2/Ar (30 mL·min^{-1}) was introduced for adsorption for 30 min, subsequently Ar was switched to remove the physically adsorbed H_2. Next 5 vol% D_2/Ar (30 mL·min^{-1}) was introduced for the H-D exchange from room temperature to 700 ℃, with a mass spectrometer monitoring the HD signal. The heating rate was 10 ℃·min^{-1}.

CO_2- and NH_3-TPD of the samples were conducted on a JW-HX 100 instrument with a Thermal Conductivity Detector (TCD). Before adsorption, 100 mg of the catalyst was pretreated at 150 ℃ in an Ar stream (30 mL·min^{-1}) for 1 h. After cooling to room temperature, the catalyst was treated with a 20 vol% CO_2/Ar or 20 vol% NH_3/Ar stream (30 mL·min^{-1}) for 30min. Subsequently, the system was purged with an Ar stream (30 mL·min^{-1}) with its temperature ramped from room temperature up to 750 ℃ at a rate of 10 ℃·min^{-1}.

H_2-TPR of the samples were conducted on a TP-5080 instrument with a TCD. 100 mg of the catalyst was pretreated at 150 ℃ in an Ar stream (30 mL·min^{-1}) for 1 h. After cooling to room temperature, the catalyst was treated with a 5 vol% H_2/N_2 at a heating rate of 10 ℃·min^{-1} from room temperature to 750 ℃.

For CO adsorption FT-IR, the sample was placed in the infrared cell, heated to 200 °C at

a rate of 5 °C/min under a flow of pure N_2 (50 mL/min), held at this temperature for 20 min, and then cooled to room temperature. Subsequently, pure CO was introduced at a flow rate of 50 mL/min for 30 min. The gas was then switched back to pure N_2, and the system was purged at 20 mL/min while the infrared signal was recorded for 60 min.

In-situ FTIR experiments of acetone adsorbed onto the catalysts were recorded on a Thermo Scientific Nicolet iS50 FTIR instrument. The samples of catalysts were dropped onto disk samples made of KBr after dissolving in ethanol and placed into a gas-solid cell. A N_2 stream (30 mL·min^{-1}) was introduced to pretreat the catalysts for 30 min at 100 °C. The heating rate was 10 °C·min^{-1}. The background spectrum was collected when the gas-solid cell was cooled to room temperature, and 10 μL acetone was added to the surface of the samples. Continue to use pure N_2 as the desorption gas at room temperature and the FTIR spectra were recorded continuously until the physically adsorbed acetone was completely desorbed and the spectra no longer changed. FTIR spectra were continuously recorded throughout the process.

Evaluation of the Catalytic Performance. The catalytic test was performed in a 50 mL stainless steel autoclave with a pressure gauge and a magnetic stirrer. Typically, the autoclave was charged with catalyst and 10 mL of acetone. 100 μL of N-heptane was also added to the autoclave as an internal standard. Before the reaction, the autoclave was purged with low-velocity H_2 for 30 s, followed by pressurizing with H_2 to reaction pressure. Then, the autoclave was heated to reaction temperature with a stirring speed of 800 r·min^{-1}. After reaction, the liquid products were separated from the catalyst by centrifugation, and quantitatively analyzed using a GC-2030 AM instrument produced by Shimadzu Corporation. Acetone conversion and selectivity of the products were defined as follows:

$$acetone\ conversion\ (\%) = \frac{acetone(inlet) - acetone(outlet)}{acetone(inlet)} \times 100\%$$

$$selectivity\ of\ products\ (\%) = \frac{acetone(converted\ to\ the\ product)}{acetone(inlet) - acetone(outlet)} \times 100\%$$

$$TOF = \frac{n_{ace} X Y_{MIBK} M_{Ni}}{g w_{Ni} t \times 100\%}$$

TOF — Turnover frequency (h^{-1});

n_{ace} — The molar amount of acetone added (mol);

X — The conversion of acetone (%);

Y_{MIBK} — The selectivity of MIBK (%);

M_{Ni} — The molar mass of Ni (g/mol);

g — The mass of input catalyst (g);

w_{Ni} — The mass fraction of Ni in the catalyst (%);

t — Reaction time (h).

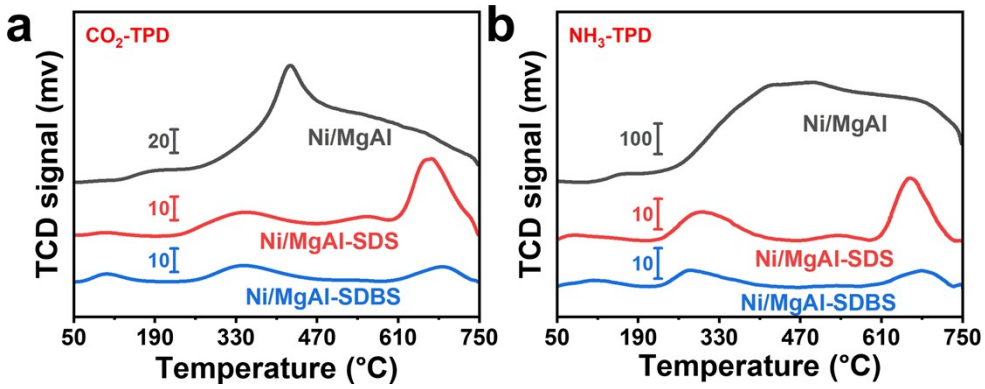

Figure S1 (a) CO_2-TPD and (b) NH_3-TPD of Ni/MgAl, Ni/MgAl-SDS and Ni/MgAl-SDBS catalysts.

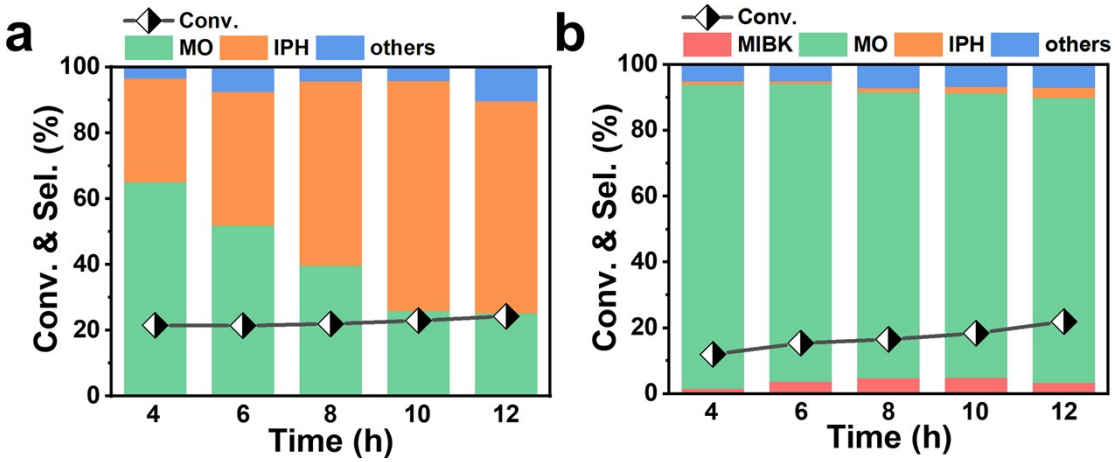

Figure S2 Time-dependent catalytic performance of (a) Ni/MgAl and (b) Ni/MgAl-SDS catalysts for acetone conversion. Reaction conditions: 160 ℃, 4 MPa, 0.15 g catalyst.

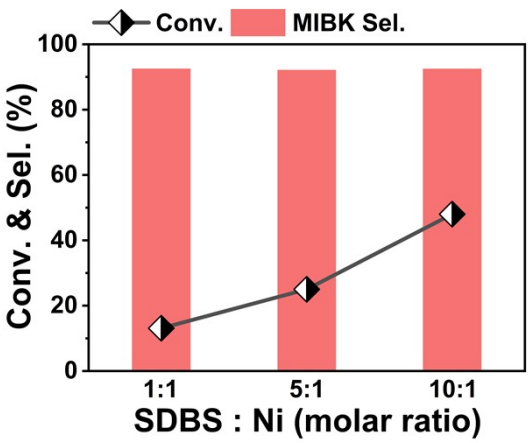

Figure S3 Catalytic performance test of different SDBS : Ni molar ratios. Reaction conditions: 160 °C, 4 MPa, 8 h, 0.15 g catalyst.

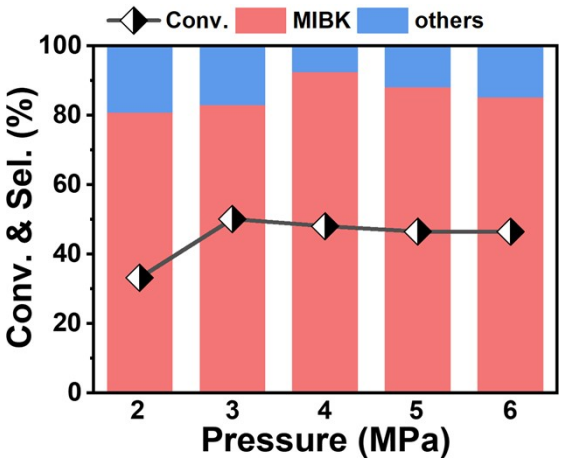

Figure S4 Pressure-dependent catalytic performance of Ni/MgAl-SDBS catalyst for acetone conversion. Reaction conditions: 160 ℃, 8 h, 0.15 g catalyst.

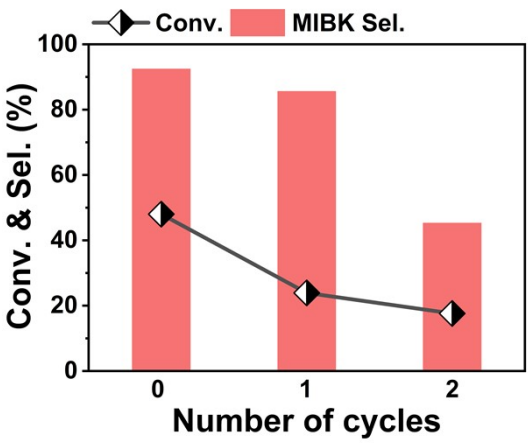

Figure S5 Cyclic stability test of Ni/MgAl-SDBS. Reaction conditions: 160 °C, 4 MPa, 8 h, 0.15 g catalyst.

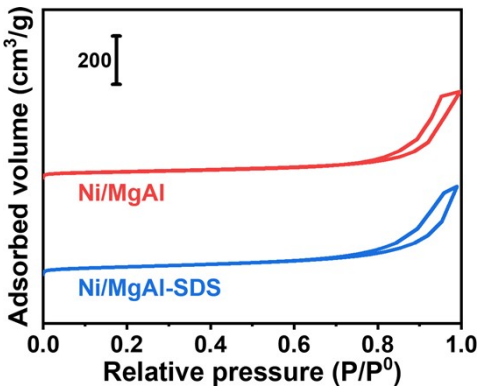

Figure S6 N_2 adsorption-desorption isotherms of Ni/MgAl and Ni/MgAl-SDS catalysts.

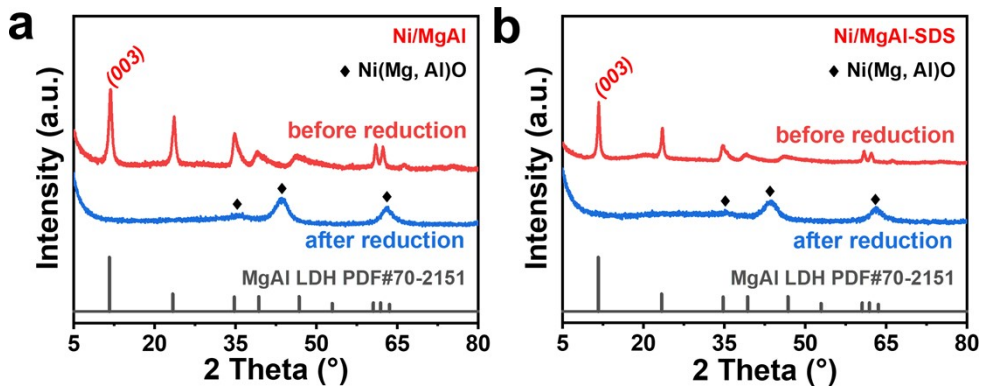

Figure S7 XRD patterns of (a) Ni/MgAl and (b) Ni/MgAl-SDS catalysts before and after reduction.

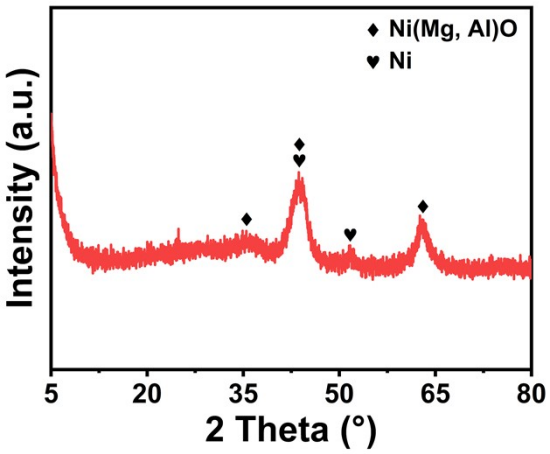

Figure S8 XRD patterns of spent Ni/MgAl-SDBS.

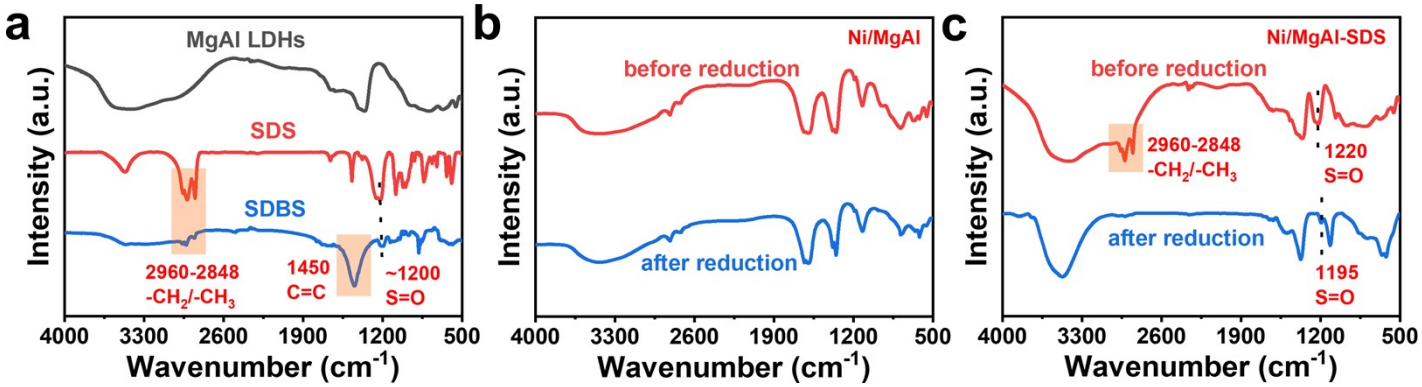

Figure S9 FTIR spectra of (a) MgAl LDHs, SDS, and SDBS; (b) Ni/MgAl before and after reduction and (c) Ni/MgAl-SDS before and after reduction.

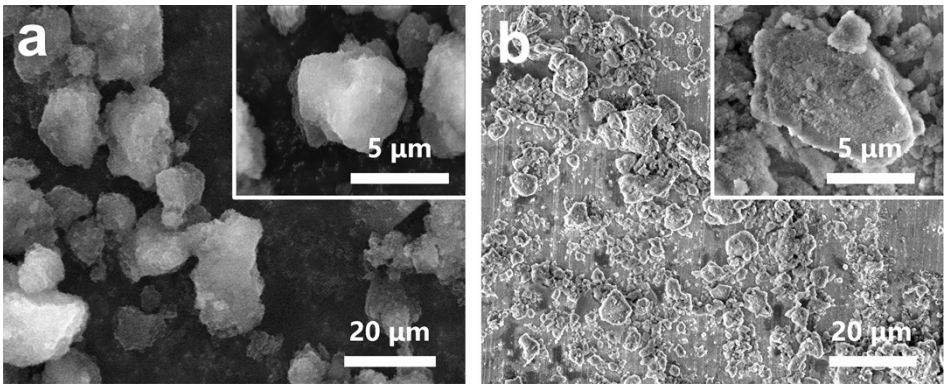

Figure S10 SEM images of (a) Ni/MgAl and (b) Ni/MgAl-SDS.

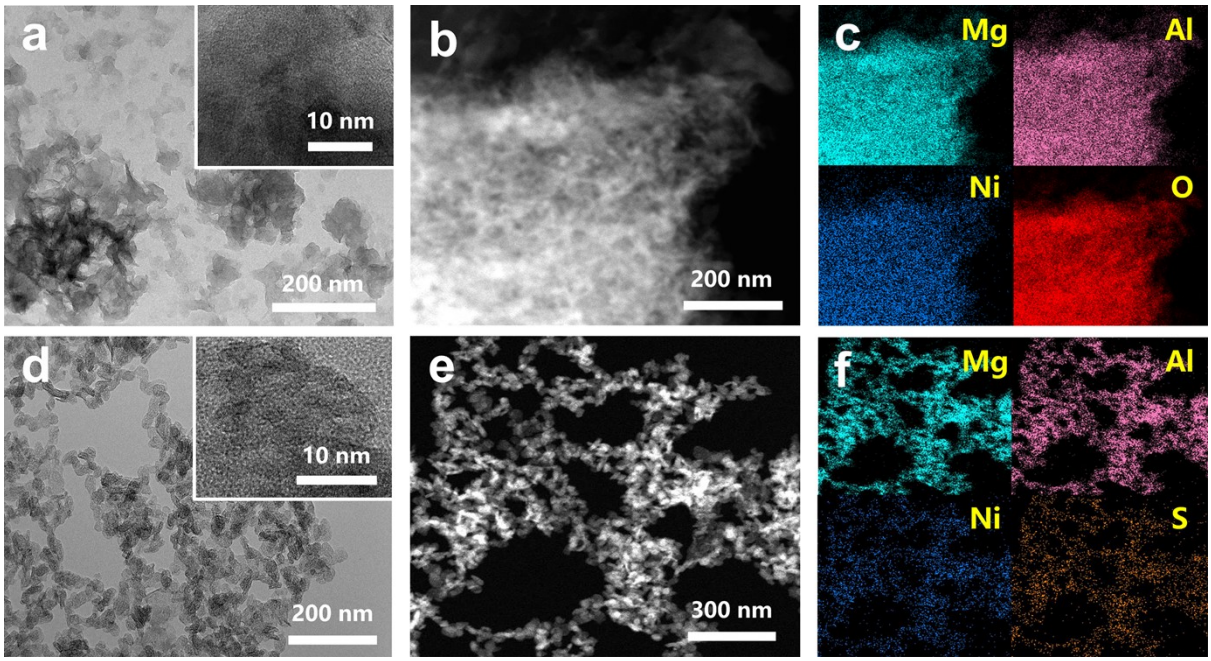

Figure S11 (a) TEM image of Ni/MgAl. (b) TEM image and (c) corresponding element mappings of Ni/MgAl. (d) TEM image of Ni/MgAl-SDS. (e) TEM image and (f) corresponding element mappings of Ni/MgAl-SDS.

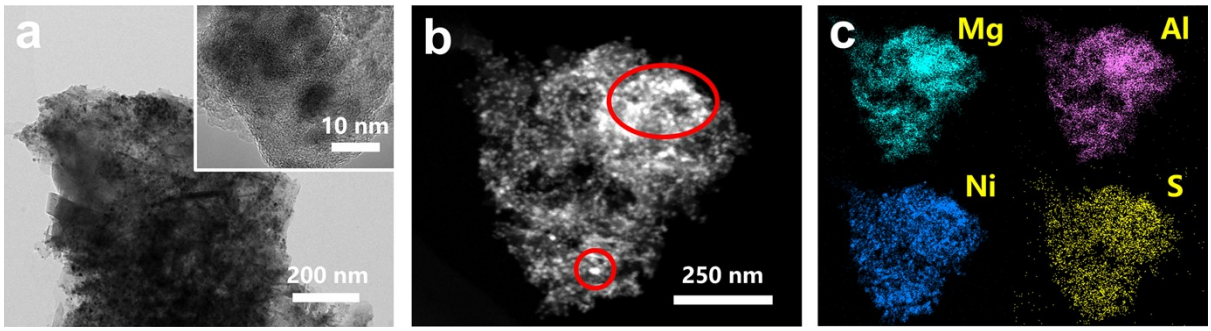

Figure S12 TEM image and corresponding element mappings of spent Ni/MgAl-SDBS.

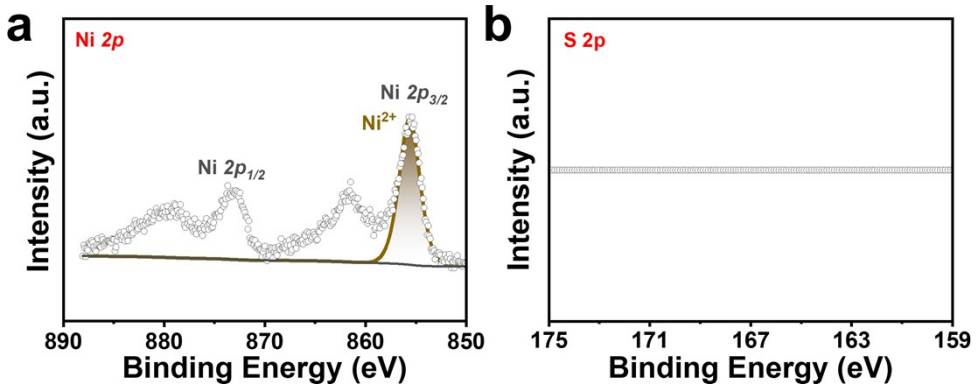

Figure S13 (a) Ni 2p and (b) S 2p XPS profiles of Ni/MgAl catalyst.

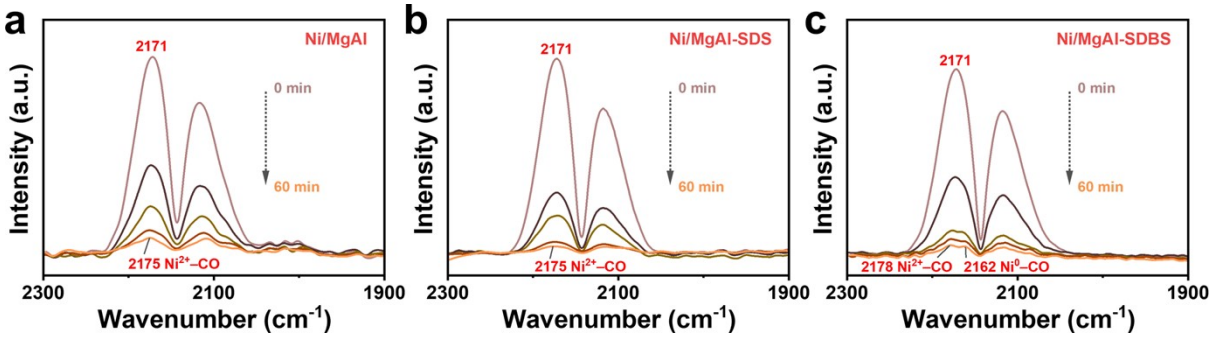

Figure S14 CO adsorption FT-IR spectra of (a) Ni/MgAl, (b) Ni/MgAl-SDS, and (c) Ni/MgAl-SDBS.

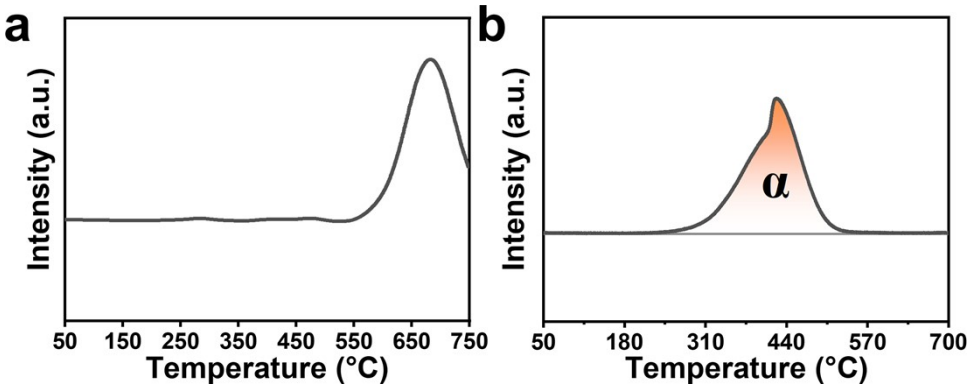

Figure S15 (a) H_2-TPR and (b) H_2-D_2 exchange of Ni/MgAl catalyst.

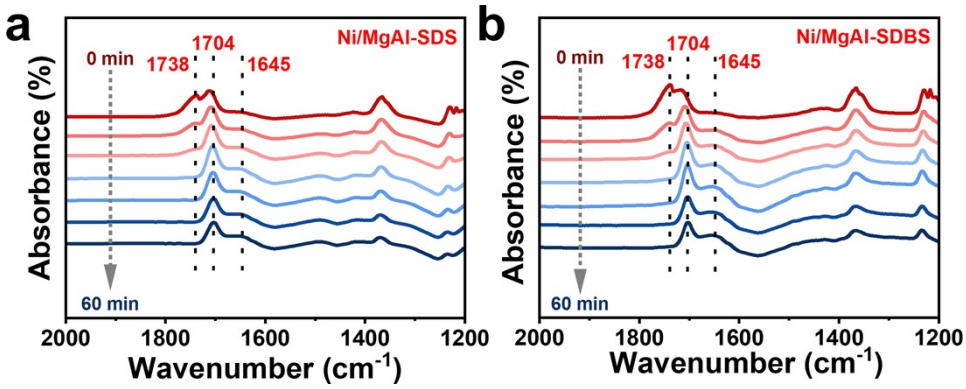

Figure S16 In-situ FTIR patterns of (a) Ni/MgAl-SDS and (b) Ni/MgAl-SDBS catalysts.

Table S1 Comparative catalytic performances between Ni/MgAl-SDBS and non-noble metal-based catalysts previously reported for the conversion of acetone to MIBK.

Catalyst	MIBK Selectivity (%)	TOF (h^{-1})	Ref.
Ni/MgAl-SDBS	92.45	29.54	this work
Ni/CeO_2	56.0	27.94	[1]
Cu-Al mixed oxide	74.0	2.62	[2]
Ni/MO5Imp	32.0	16.79	[3]
Ni/TiO_2	1.3	0.0009	[4]
Ni/C	62.0	0.92	[5]
Cu/C	13.0	0.34	[5]
Cu/A15	8.0	0.18	[6]
Cu/Dow2	5.0	0.18	[6]
Cu/MgO	50.0	6.25	[7]
Cu/HAP	93.0	19.03	[8]
Ni/Al_2O_3	96.0	25.14	[9]

Table S2 Specific surface area and pore characteristics of Ni/MgAl, Ni/MgAl-SDS, and Ni/MgAl-SDBS catalysts.

Sample	BET surface area (m^2/g)	Pore volume (cm^3/g)	Pore size (Å)
Ni/MgAl	101.0	0.558	221.0
Ni/MgAl-SDS	121.3	0.568	187.1
Ni/MgAl-SDBS	104.4	0.509	195.1

Table S3 The assignment of vibrational mode detected in FTIR spectra of Ni/MgAl, Ni/MgAl-SDS, and Ni/MgAl-SDBS catalysts.

Vibrational mode	Vibrational mode in this work (cm^{-1})	Vibrational mode in literature (cm^{-1})	Ref.
ν (-OH)	3470	3448	10
ν (-CH_2/CH_3)	2848-2960	2851-2922	11
δ (H_2O)	1635	1630	10
ν (C=C)	1450	1450	12
δ (C-H)	1400	1406	13
ν (CO_3^{2-})	1350	1360	10
ν (S=O)	1195-1220	1215	12
ν (C-H)	1115	1130	14
ν (Metal-O)	<1000	<1000	15

Table S4 The loadings of Ni and S in Ni/MgAl, Ni/MgAl-SDS, and Ni/MgAl-SDBS catalysts.

Sample	Ni content (wt.%)	S content (wt.%)
Ni/MgAl	4.100	0
Ni/MgAl-SDS	6.020	2.967
Ni/MgAl-SDBS	10.606	1.007

Table S5 Parameter comparison of Ni/MgAl, Ni/MgAl-SDS and Ni/MgAl-SDBS.

Catalyst	Ni^0 molar ratio	The area of NH_3-TPD*	Ni^0 molar ratio / The area of NH_3-TPD	The selectivity of MIBK (%)	The yield of MIBK ($mol \cdot h^{-1} \cdot g_{cat}^{-1}$)
Ni/MgAl	0	100	0	0	0
Ni/MgAl-SDS	0	2.05	0	4.70	0.167
Ni/MgAl-SDBS	0.498	1.37	0.364	92.45	3.725

* For the convenience of comparison, we set the NH_3-TPD integral area of Ni/MgAl to 100

Table S6 The assignment of vibrational mode detected in in-situ FTIR spectra of Ni/MgAl-SDS and Ni/MgAl-SDBS catalysts.

Vibrational mode	Vibrational mode in this work (cm^{-1})	Vibrational mode in literature (cm^{-1})	Ref.
ν (C=O) in the gas-phase acetone	1738	1740	16
ν (C=O) in the adsorbed acetone	1704	1710	16
ν (O-H) in the adsorbed acetone	1645	1639	17
δ (-CH_2-)	1492	1495	18
δ_{as} (-CH_3)	1424-1428	1419-1421	19
δ_s (-CH_3)	1365	1366	19
ν (C-C)	1233	1228-1236	19

Supplementary Reference

1 P. V. R. Rao, V. P. Kumar, G. S. Rao and K. V. R. Chary, *Catal. Sci. Technol.*, 2012, **2**, 1665.

2 S. Basu, J. J. Sarkar and N. C. Pradhan, *Catal. Today*, 2022, **404**, 182–189.

3 A. C. C. Rodrigues, J. L. F. Monteiro and C. A. Henriques, *Comptes Rendus Chim.*, 2009, **12**, 1296–1304.

4 J. Quesada, L. Faba, E. Díaz and S. Ordóñez, *J. Catal.*, 2019, **377**, 133–144.

5 G. Waters, O. Richter and B. Kraushaar-Czarnetzki, *Ind. Eng. Chem. Res.*, 2006, **45**, 6111–6117.

6 E. Canadell, J. H. Badia, R. Soto, J. Tejero, R. Bringué and E. Ramírez, *Top. Catal.*, 2025, **68**, 59–81.

7 V. Chikán, Á. Molnár and K. Balázsik, *J. Catal.*, 1999, **184**, 134–143.

8 K. Grzelak, M. Trejda and A. Riisager, *ChemSusChem*, 2022, **15**, e202102012.

9 S. Narayanan and R. Unnikrishnan, *Appl. Catal. Gen.*, 1996, **145**, 231–236.

10 X. Meng, Y. Yang, L. Chen, M. Xu, X. Zhang and M. Wei, *ACS Catal.*, 2019, **9**, 4226–4235.

11 P. Sanati-Tirgan, H. Eshghi and A. Mohammadinezhad, *Nanoscale*, 2023, **15**, 4917–4931.

12 M. Bouraada, M. S. Ouali and L. C. De Ménorval, *J. Saudi Chem. Soc.*, 2016, **20**, 397–404.

13 Z. Yan, Z. Yang, Z. Xu, L. An, F. Xie and J. Liu, *J. Colloid Interface Sci.*, 2018, **524**, 306–312.

14 P. Huang, A. Liu, L. Kang, M. Zhu and B. Dai, *New J. Chem.*, 2018, **42**, 12830–12837.

15 Y. Zou, P. Wang, W. Yao, X. Wang, Y. Liu, D. Yang, L. Wang, J. Hou, A. Alsaedi, T. Hayat and X. Wang, *Chem. Eng. J.*, 2017, **330**, 573–584.

16 K. Liu, Y. Sun, J. Feng, Y. Liu, J. Zhu, C. Han, C. Chen, T. Bao, X. Cao, X. Zhao, Y. Yang and G. Zhao, *Chem. Eng. J.*, 2023, **454**, 140059.

17 M. D. Hernández-Alonso, I. Tejedor-Tejedor, J. M. Coronado, M. A. Anderson and J. Soria, *Catal. Today*, 2009, **143**, 364–373.

18 A. H. Alminshid, M. N. Abbas, H. A. Alalwan, A. J. Sultan and M. A. Kadhom, *Mol. Catal.*, 2021, **501**, 111333.

19 H. Alalwan and A. Alminshid, *Spectrochim. Acta. A. Mol. Biomol. Spectrosc.*, 2020, **229**, 117990.